Hindawi
International Journal of Corrosion
Volume 2019, Article ID 8517648, 8 pages
https://doi.org/10.1155/2019/8517648

Research Article

Isothermal Oxidation Behaviour of 69.5Fe-14Ni-9Al-7.5Cr Alloy at High Temperatures

Eddy Agus Basuki,[1] **Dedi Chandra Nababan**,[1] **Fadhli Muhammad**,[1] **Akhmad Ardian Korda**,[1] **and Djoko Hadi Prajitno**[2]

[1]*Department of Metallurgical Engineering, Faculty of Mining and Petroleum Engineering, Bandung Institute of Technology, Jl. Ganesha No. 10, Bandung 40132, Indonesia*
[2]*Nuclear Technology Center for Materials and Radiometry, National Atomic Agency of Indonesia, Jl. Taman Sari No. 71, Bandung 40132, Indonesia*

Correspondence should be addressed to Eddy Agus Basuki; basuki@mining.itb.ac.id

Received 7 September 2018; Revised 11 December 2018; Accepted 30 December 2018; Published 3 February 2019

Academic Editor: Flavio Deflorian

A series of experiments have been conducted to study the resistance of isothermal oxidation in 69.5Fe-14Ni-9Al-7.5Cr (% wt) alloys with some temperature variations of 800, 900, and 1000°C and each temperature is tested for 1, 10, 50, and 150 hours. Based on the analysis conducted on the test results, it is known that the higher the oxidation temperature, the faster the oxidation rate. As for the duration of oxidation, the longer the testing time is, the smaller the weight change per unit sample area is, indicated by a sloping graph. The oxide products found in this study were Fe_2O_3, Fe_3O_4, α-Al_2O_3, NiO, Cr_2O_3, and $NiCr_2O_4$. The rate of oxidation of this alloy at each temperature follows a logarithmic equation indicating that the oxide layer formed is very thin and can protect the metal surface well. The oxidation rate constants at temperatures of 800, 900, and 1000°C are 5.15E-05, 5.57E-05, and 6.74E-05 gr.cm^{-2}, respectively.

1. Introduction

Relatively high global energy demand has forced the policies to increase the power plant efficiency, especially for those use fossil fuels, such as coal-based steam power plants. Increasing power plant efficiency can be achieved by increasing the pressure and temperature of the steam. Consequently, materials with capability to be used at higher temperature are demanding. Such materials should have high creep resistance as well as high temperature corrosion and oxidation.

The advanced ferritic steels with alloying elements of Ni, Al, and Cr have been the alternative materials used in some parts of power plant construction due to the combination of low thermal expansion coefficient and relatively low price compared with nickel-based super alloys [1]. In addition, these materials have high temperature strength resulted from the occurrence of coherent precipitate B2-FeNi(Al) in the ferrite matrix of α [2, 3]. This microstructure is essentially similar to that found in nickel-based superalloys, but these later alloys have austenitic matrix of γ. Relatively slight difference in lattice parameter α-Fe (A2) and precipitates NiAl (B2) as well as similar crystal structures of both phases provides the ordering and coherency that provide high strength [4]. Therefore, the strength or creep resistance of the materials increases with the volume fraction of B2-FeNi(Al) precipitates [5].

Stallybrass and coworkers [6] have studied the Fe-Ni-Al-Cr alloys and referred to the pseudobinary phase diagram of Fe+2.5 at.% Al – NiAl+1.25 at.% Al. The chemical composition was selected to produce various volume fraction of the alloys. Alloys with typically containing B2-FeNi(Al) dispersed homogeneously in the ferrite matrix of α are then known as ferritic superalloys [7]. These alloys have been recently studied, mostly focused on the mechanical properties as well as microstructural changes at high temperatures [8–10]. Various mixtures of phases in different quaternary alloy systems of Fe-Ni-Cr-Al at 900°C have been investigated by Yin *et al.* [11]. Three phases of α-ferrite, β-FeNi(Al), and

Table 1: Raw material proportion for alloy making.

Elements	Weight %	Raw materials	Theoretical weight (gram)	Actual weight (gram)
Fe; Ni	50; 14	FeNi shot	12.78	12.7912
Fe	19,5	Fe chip	4.00	3.9904
Al	9	Granulated Al	1.8	1.8150
Cr	7,5	Cr	1.5	1.5100

γ-austenite were identified; alloy 70Fe3Cr12Al15Ni gave three phase of $\alpha+\beta+\gamma$, while alloy 70Fe6Cr15Al9Ni produced $\alpha+\beta$. Alloy containing two phase of $\beta+\gamma$ had chemical composition of 70Fe3Cr9Al18Ni. Addition of Ni increases the toughness and high temperature strength, while addition of both Ni and Al promotes the precipitates of B2-FeNi(Al) that increases the creep resistance of the alloys [12]. Therefore, the strength and creep resistance of the alloy increase with increasing the volume fraction of B2-FeNi(Al).

Oxidation resistance of the ferritic alloys for high temperature application relies on the formation of a continuous slow growing protective scale based on Al_2O_3 [13]. Chromium addition can improve the high temperature oxidation as Cr can act as oxygen getter that reduces the critical aluminium content for external continuous layer of Al_2O_3 [14]. Therefore, in the case of B2-FeNi(Al) strengthened ferritic alloys, the involvement of Cr in the alloys can decrease the potency for B2 in substrate underneath the scale to dissolve.

Recently, we have developed a ferritic alloy with chemical composition of 69.5Fe-14Ni-9Al-7.5Cr that has precipitates of B2-FeNi(Al) dispersed homogeneously in the ferrite matrix of α. The alloy contains "bone-like" precipitates of B2, dispersed along certain crystallography orientation. The alloy is intended to be used for high temperature components of power generators, especially coal-based steam power plants. Most high temperature components used in such operations require high oxidation resistant properties. This paper discussed the results of isothermal oxidation behaviour of the alloy at 800, 900, and 1000°C.

2. Experimental Works

The alloy of this study had a chemical composition of 69.5Fe-14Ni-9Al-7.5Cr (otherwise stated the composition is in weight percent) or is equivalent with 72.74 at%Fe,15.40 at%Ni, 4.55 at% Al, and 7.31 at.% Cr. The raw materials for alloy making were low carbon ferronickel-shot obtained from PT ANTAM (Persero) Tbk., pure aluminium (>99%) obtained from PT. Inalum, and pure chromium and iron obtained from Sigma Aldrich. To obtain chemical composition of the alloy, raw material proportion was set up as shown in Table 1. The raw materials were melted in an argon purged single mini electric arc furnace at 220V and 75-90A for 2 minutes. In order to produce homogeneous alloy buttons, each with 20 grams weight, repeated melting was carried out for 5 times. Further homogenization was done by heating the alloy button at 1100°C for 24 in a horizontal tube furnace purged with high purity argon.

The homogenized alloy buttons were then cut to produce samples of 6 mm x 6 mm x 1 mm in size using low speed diamond cutter. The samples were polished finish at 2000 grit and cleaned in acetone using an ultrasonic cleaner. Weighing and surface area measurement of each sample were carried out prior to oxidation test. Isothermal oxidation tests were carried out by heating the samples at 800, 900 dan 1000°C for 1, 10, 50, and 150 hrs. in a tube heat resistance electric furnace. Weighing of the oxidized samples was done to obtain the weight change of each sample. Microstructural analysis of the samples was carried out using optical microscope and scanning electron microscope (SEM) in which an energy dispersive X-ray spectroscopy is attached. To reveal the microstructure of the substrate, the as-homogenized alloy and the oxidized samples were etched in chemical solution containing 0.1 mL HF, 3.3 mL acetate acid, 3.3 mL HNO_3, and 3.3 mL H_2O. Point-count method was used to measure the volume fraction of primary B2 precipitates in the substrate of each sample based on the SEM images. X-ray diffraction analyzer (XRD) was used to identify the oxides formed on the surface of the oxidized samples. To confirm the occurrence and distribution of different oxides in the scales, X-ray mapping was applied.

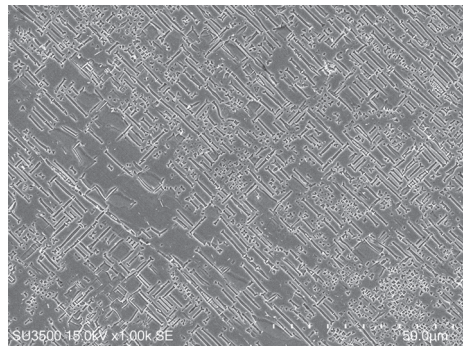

Figure 1: Dispersion of rod-like B2 (Fe,Ni)Al precipitates in the ferrite-α matrix of as-homogenized sample.

3. Results and Discussion

The as-homogenized alloy sample of 69.5Fe-14Ni-9Al-7.5Cr essentially has two phases, as shown in Figure 1. It is seen clearly that rod-like ordered B2 (Fe,Ni)Al precipitates dispersed homogeneously throughout the ferrite-α (α-Fe) matrix. Identification of these two phases was based on the EDX analysis of the samples, as shown in Figures 2 and 3. However, different from these normally rod-type precipitates in ordinary alloys, the B2 (Fe,Ni)Al precipitates in this alloy have more likely bone-type precipitates, in which epiphysis-like structures are set up on both rod tips. These type

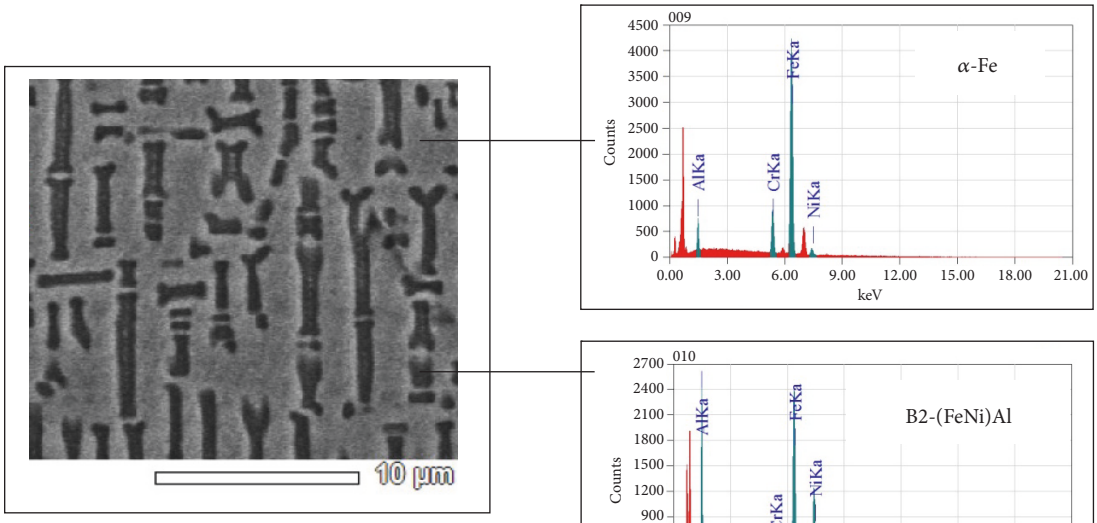

Phase	Chemical composition (at.%)			
	Fe	Ni	Al	Cr
α-Fe	65.87	6.23	16.42	11.48
B2-(Fe,Ni)Al	30.18	21.42	45.78	2.62

Figure 2: EDX analysis of phases in the sample heated at 800°C for 150 hrs.

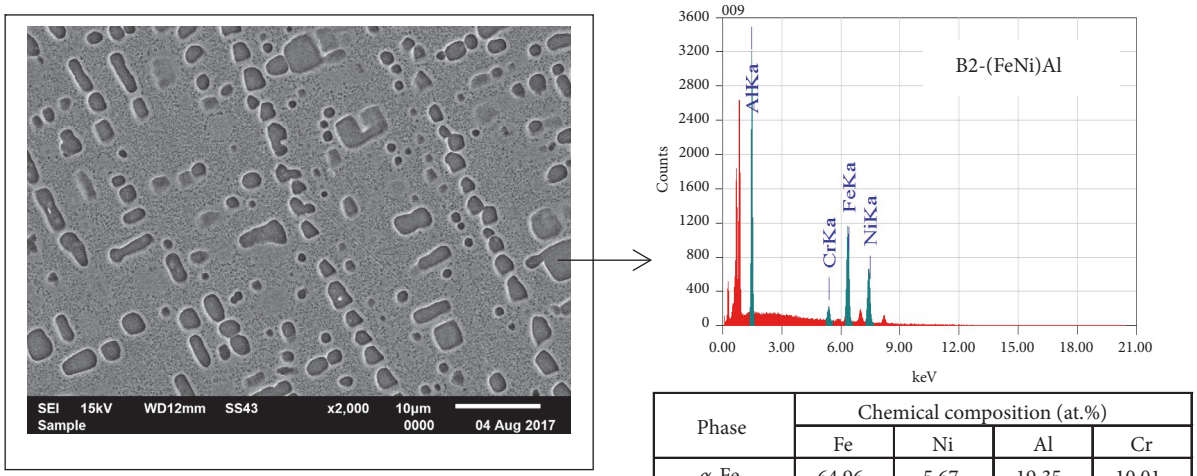

Phase	Chemical composition (at.%)			
	Fe	Ni	Al	Cr
α-Fe	64.96	5.67	19.35	10.01
B2-(Fe,Ni)Al	29.45	22.65	44.32	3.57

Figure 3: EDX analysis of phases in the substrate sample heated at 1000°C for 150 hrs.

precipitates have not been found in literatures discussing B2 contained ferritic steels. Most literatures indicate that B2 (Fe,Ni)Al precipitates have cuboidal or rounded type structures [6, 8, 9]. Heating the alloy at high temperatures changes the volume fraction, morphology, and size of the B2 precipitates. These microstructural changes occurred significantly at higher temperatures, especially at 1000°C, as seen in Figures 2 and 3. The as-homogenized particle size of B2 was about 1-2 μm in wide dimension and can reach up to more than 10 μm in length.

The volume fraction of the homogenized samples was 36.3%. Heating the alloy at different temperatures reduced the volume fraction of B2. Heating at 800, 900, and 1000°C, the volume fraction of B2 was 33.6%, 30.5, and 26.6%, respectively. Moreover, it was revealed that volume fraction of B2 precipitates decreased with time of heating, as shown in Figure 4. This decreasing volume fraction of B2 with time has been well recognized in the study of particle coarsening [15]. The stability of the B2 rods at 800°C was relatively high, as most B2 precipitates were still in rod type when the alloy was

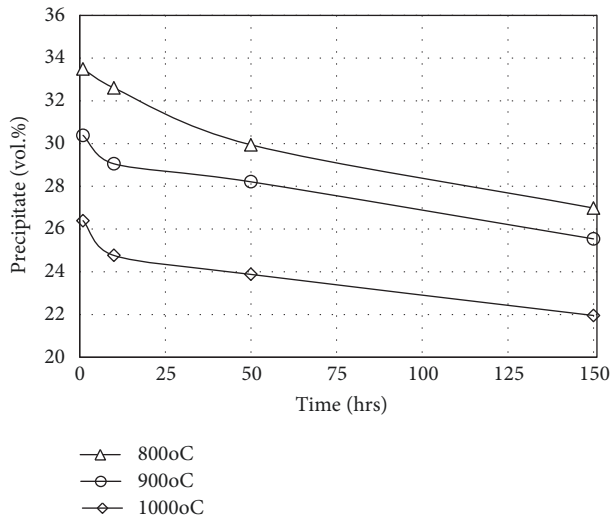

Figure 4: Percentage of B2 particles in sample substrates after heating at different temperatures and times.

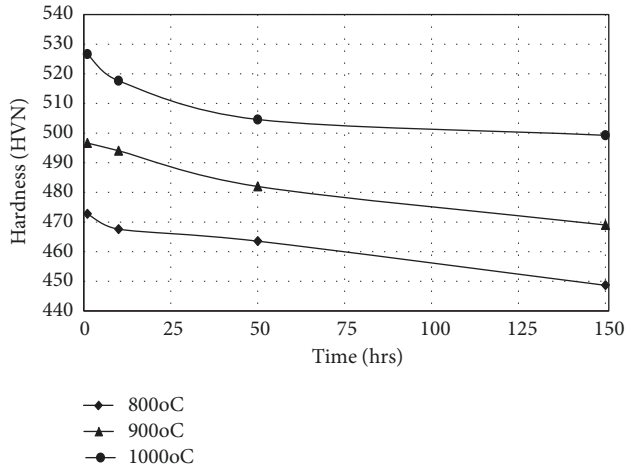

Figure 5: Hardness of the substrate in samples heated at different temperatures and times.

heated for 150 hrs. However, at 1000°C, the morphology of the B2 tended to be more rounded, due to the spheroidization of the B2 rods. These volume fraction and morphology changes of the B2 precipitates caused the hardness of the alloy to decrease, as shown in Figure 5.

Exposing the alloy samples at high temperatures at atmospheric condition caused the alloy to oxidize followed by the scale formation containing various oxides on the surface of the alloy. Figure 6 show the scales on the samples oxidized at 800, 900, and 1000°C for 150 hrs. The thickness of the scales in varies from very thin of about 2 μm in sample oxidized at 800°C up to relative thick of about 8 μm in sample oxidized at 1000°C. EDS analysis of the scales shows that the scale contains mostly aluminium oxide and chromium oxide. No B2 precipitate depleted zones underneath the scales were found indicating that aluminium content in the α-Fe matrix in all samples was adequate to provide aluminium atoms to form Al_2O_3 in the scales. Moreover, no internal oxidation was found in all samples. The XRD analysis results, shown in Figure 7, confirmed that oxides of Fe_3O_4, Fe_2O_3, Cr_2O_3, Al_2O_3, NiO, and spinel of $NiCr_2O_4$ were detected in all sample surfaces. It is believed that the outer parts of the scales were dominated by iron oxide of Fe_3O_4 and Cr_2O_3.

X-ray mapping results confirmed further that most Al and Cr contained in the scales of samples heated at 900 and 1000°C, as shown in Figures 8 and 9, respectively. A particle found in the substrate of sample oxidized at 900°C, Figure 8, did not result from internal oxidation, but an Al_2O_3 inclusion in the alloy formed during melting is expected, as it is surrounded by relatively thick B2 phase. In scale of sample oxidized at 1000°C, it was found that aluminium oxide formed in the upper part as well as lower part of the scale.

Iron oxides of Fe_2O_3, Fe_3O_4, and FeO are believed to be formed at the first stage of oxidation at all temperatures studied [16, 17], as the alloy rich in iron, even though these oxides are thermodynamically less stable compared with Al_2O_3 and Cr_2O_3. With time, underneath iron oxides depleted in Fe and consequently enrich the Ni, Al, and Cr. Even though nickel content is higher in the alloy compared with aluminium, thermodynamically Al_2O_3 is much stable than NiO. Enrichment of Cr in this region would drive formation of Cr_2O_3. However, Cr_2O_3 is less stable than Al_2O_3. Therefore, Al_2O_3 would form immediately bellow iron oxides scale. Formation of this aluminium oxide reduced inward diffusion of oxygen to the alloy surface as the Fe^{n+} ions have larger size compared with other anions [13], making the outward diffusion of iron ions to the oxygen rich regions decrease. The growth of Al_2O_3 layer caused depletion aluminium content in the alloy below the scale. Consequently, as the Cr and Ni content increased, Cr_2O_3 and NiO would form, dominated by chromia formation. Formation of Cr_2O_3 reduces the oxygen pressure on the alloy-scale interface and reduces the possibility of iron oxides to form further [18]. NiO normally formed by outward diffusion of cation [19]. However, relatively larger size of Ni^{2+} and higher Gibbs free energy for NiO formation a layer of NiO would not be possible to form, except dispersion of NiO particles in a layer of Cr_2O_3. Reaction or mutual dissolution of these two oxides might produce spinel of $NiCr_2O_4$ in this layer as also found in the study of Dudziak etal [20] in Cr-rich FeNi alloys of Hayness 6 [17] but at lower temperature of 750°C. Bensch etal [21] found this type of spinel in GTD111 Ni-base superalloy oxidized at 900°C. This is basically the result of reaction between these two oxides. Depletion of Cr and Ni contents in the alloy underneath Cr and Ni oxides induced the formation of aluminium oxide or alumina layer.

The oxidation resistance of the alloy at 800, 900, and 1000°C can be obtained from the weight gain plot with time, as shown in Figure 10. It is seen that the thickness of the scale increases rapidly at the beginning, indicating that the oxidation rate was very slow at the early stage of oxidation. With longer time, the rate of oxidation, represented by the slope of the curves, decreases with times. The kinetic characteristic of the oxidation can be analyzed from the weight gain data and three possible equations were analyzed by (1) plotting linearly of x with time for linier rate, (2) x

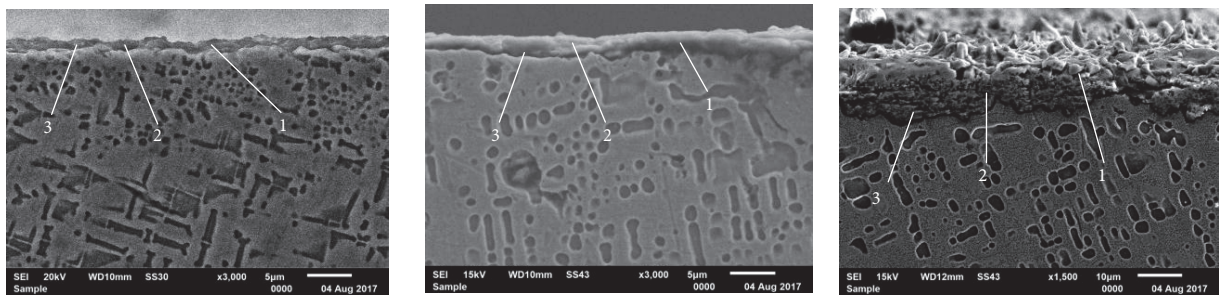

Point	Chemical composition (at.%)				
	Fe	Ni	Al	Cr	O
1	11.92	0.27	58.85	4.82	24.14
2	33.11	0.89	29.5	13.7	22.83
3	21.99	0	40.55	16.67	20.79

(a)

Point	Chemical composition (at.%)				
	Fe	Ni	Al	Cr	O
1	2.86	0.05	43.86	4.8	48.43
2	0.29	0	33.51	0.15	66.05
3	1.59	0.1	41.53	0.6	56.18

(b)

Point	Chemical composition (at.%)				
	Fe	Ni	Al	Cr	O
1	0.28	0.03	35.17	0.05	64.48
2	1.22	0	34.47	2.99	61.32
3	0.14	0	33.01	0.1	66.75

(c)

Figure 6: Scale formed on the samples exposed within 150 hrs. at (a) 800°C, (b) 900°C, and (c) 1000°C.

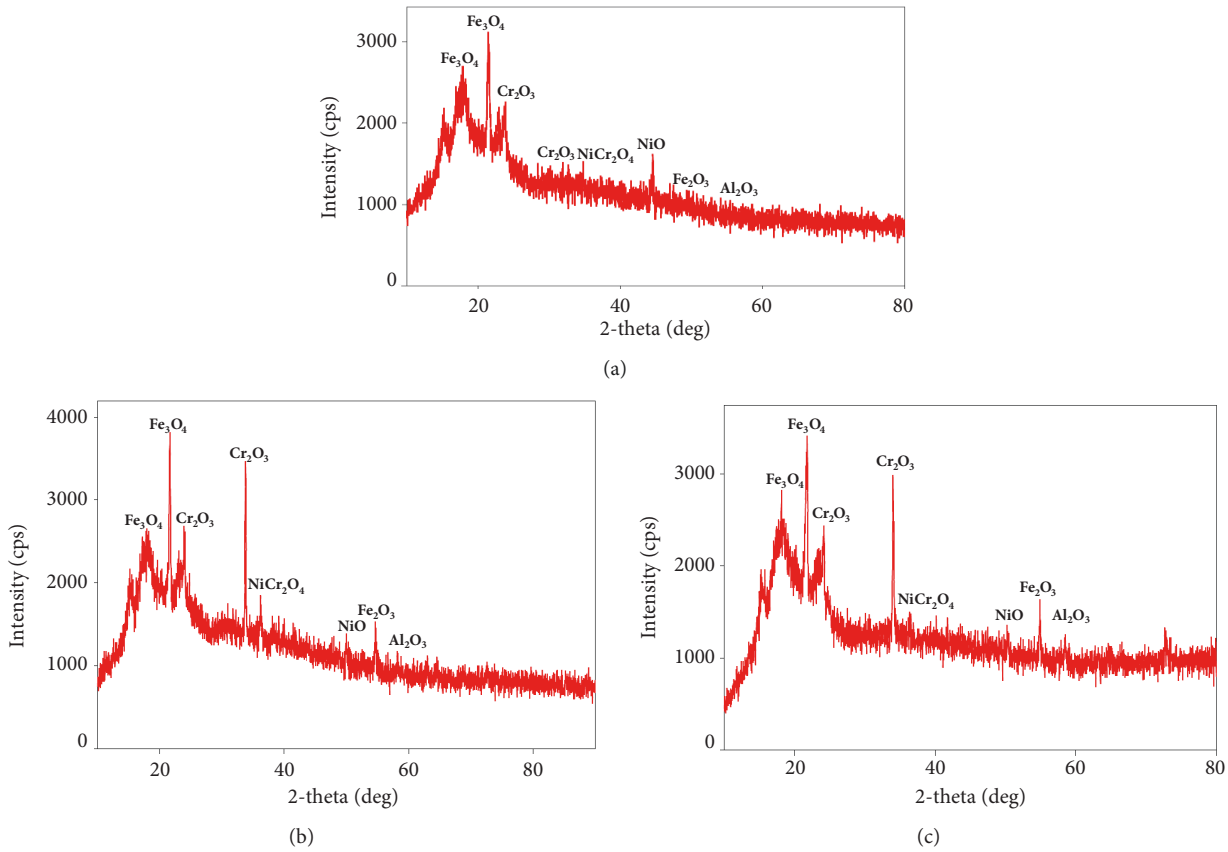

Figure 7: X-ray diffraction patterns of samples oxidized within 150 hrs. at (a) 800°C, (b) 900°C, and (c) 1000°C.

with log (t) for logarithmic rate, and (3) x^2 to t for parabolic rate. Table 2 shows all possible equations with various R^2. It is found that, at all temperatures studied, the oxidation kinetics follow logarithmic rate. This indicates that the oxidation rates of the alloy were very slow, and the oxides formed are relatively compact [20]. The values of the logarithmic rate constants for oxidation at 800, 900, and 1000°C are 5.15E-05 gr.cm^{-2}, 5.57E-05 gr.cm^{-2}, and 6.74E-05 gr.cm^{-2}, respectively, showing that the oxidation rate increased with temperatures.

Kofstad [22] provided the method to evaluate the oxidation rate equation using double-logarithmic plot by plotting log dw/A versus log t. This method can be used to see the fitting of the gradient, or m, of each resulted line where 1,

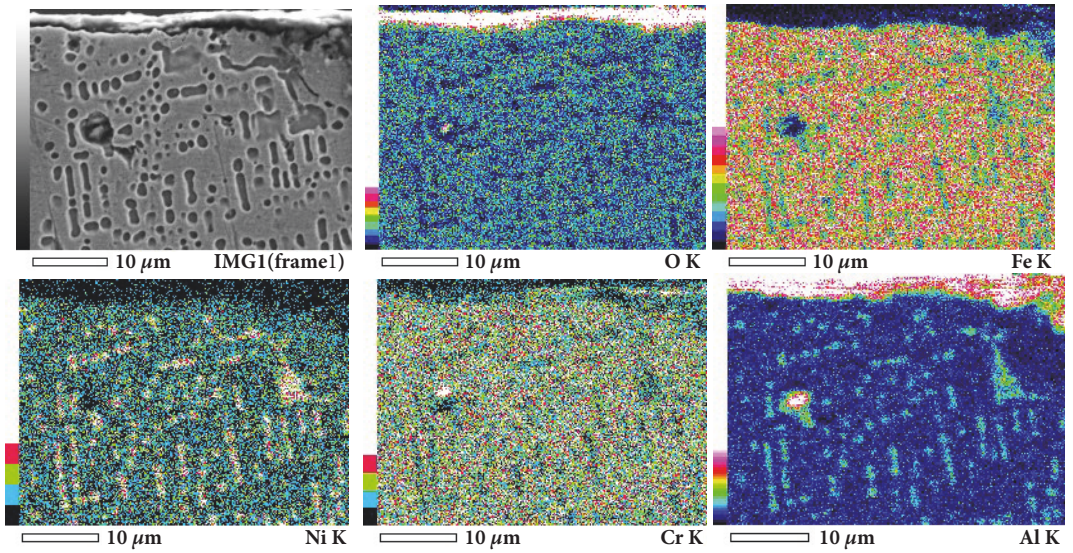

Figure 8: X-ray mapping of scale on sample oxidized at 900°C for 150 hrs.

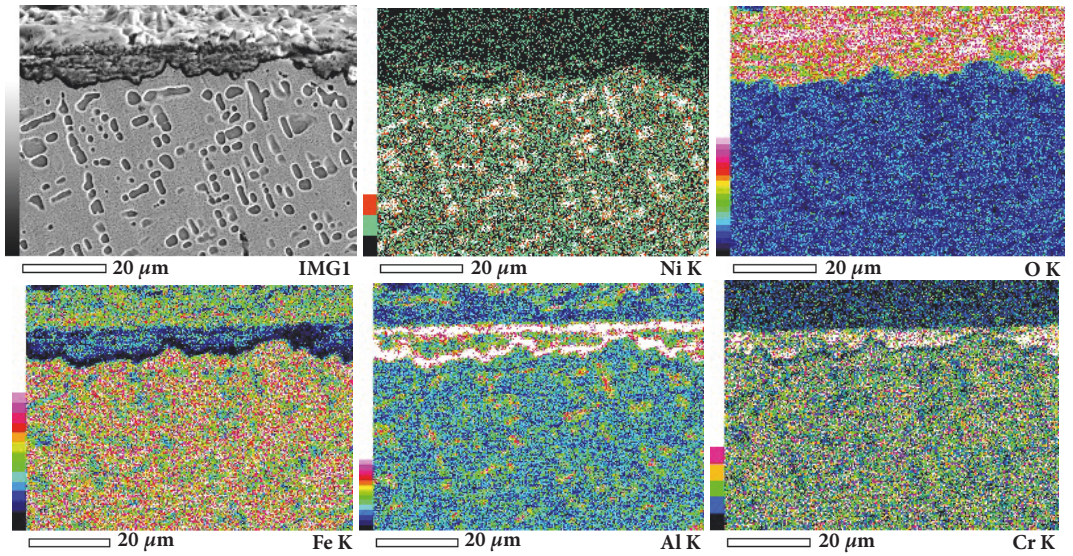

Figure 9: X-ray mapping of scale on sample oxidized at 1000°C for 150 hrs.

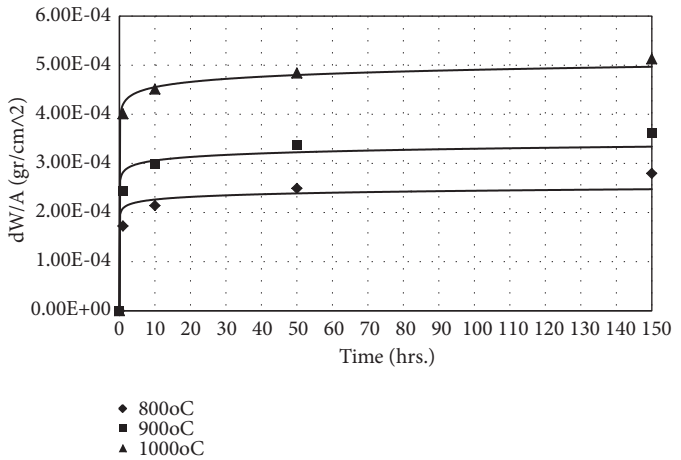

Figure 10: Weight change of samples oxidized at different temperatures and times.

Table 2: Oxidation rate equations and rate constants of samples at different temperatures.

Temperature	Oxidation rate	Equations	K	R^2
800 ˚C	Linier	x = 6E-07t + 0.0002	6E-07 $gr.cm^{-2}.hr^{-1}$	0,7961
	Parabolic	x^2 = 3E-10t + 4E-08	3E-10 $gr^2.cm^{-4}.hr^{-1}$	0,8485
	Logarithmic	x = 5.1542E-05 log (t+0.6537) + 1.6124E-04	5.15E-05 $gr.cm^{-2}$	0,9987
900 ˚C	Linier	x = 6E-07t + 0.0003	6E-07 $gr.cm^{-2}.hr^{-1}$	0,7117
	Parabolic	x^2 = 4E-10t + 8E-08	4E-10 $gr^2.cm^{-4}.hr^{-1}$	0,7568
	Logarithmic	x = 5.5723E-05 log (t+0,0777) + 2.4178E-04	5.57E-05 $gr.cm^{-2}$	0,9941
1000 ˚C	Linier	x = 6E-07t + 0.0004	6E-07 $gr.cm^{-2}.hr^{-1}$	0,7301
	Parabolic	x^2 = 6E-10t + 2E-07	6E-10 $gr^2.cm^{-4}.hr^{-1}$	0,7593
	Logarithmic	x = 6.7479E-05 log (t+9.4928) + 3.6415E-04	6.74E-05 $gr.cm^{-2}$	0,9958

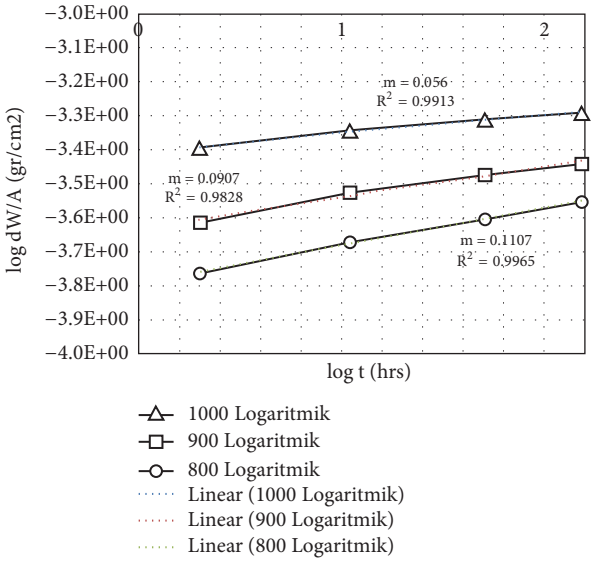

Figure 11: Double-logarithmic plot results.

2, and 3 are for linear, parabolic, or cube, respectively. The lines from plot results, as shown in Figure 11, indicate that no m values fit with the values for linear, parabolic, or cube. Therefore, logarithmic rate behaviour is confirmed for the oxidation behaviour of the 69.5Fe-14Ni-9Al-7.5Cr containing B2 (Fe,Ni)Al precipitates at 800, 900, and 1000˚C. The oxides of iron oxide formed at the early stage of oxidation grow very fast and followed by very slow growing of alumina and spinel that acted as compact thin scale of less than 5 μm and significantly reduced the rate of further oxidation.

4. Conclusion

The homogenized 69.5Fe-14Ni-9Al-7.5Cr alloy had B2 (Fe,Ni)Al precipitates dispersed homogeneously throughout the ferrite-α (α-Fe) matrix. The morphology of B2 was found as bone-type but tended to change into rounded type when heated at higher temperatures and longer times. In addition, after heating, the volume fraction of the B2 precipitates decreased causing the hardness of the alloy reduced. Scale formed on the surface of the samples consisted of oxides of Fe_2O_3, Fe_3O_4, α-Al_2O_3, NiO, Cr_2O_3, and $NiCr_2O_4$, but dominated by α-Al_2O_3 and Cr_2O_3. Due to relatively thin layer of oxide scales in order of 2 up to 8 μm, logarithmic type kinetics was observed for all oxidation temperatures. Oxidation rate constant for 800, 900, and 1000˚C was, respectively, 5.15E-05 $gr.cm^{-2}$, 5.57E-05 $gr.cm^{-2}$, and 6.74E-05 $gr.cm^{-2}$.

Data Availability

The data used to support the findings of this study are available from the corresponding author upon request.

Conflicts of Interest

The authors declare that they have no conflicts of interest.

References

[1] Z. B. Jiao, J. H. Luan, M. K. Miller, Y. W. Chung, and C. T. Liu, "Co-precipitation of nanoscale particles in steels with ultra-high strength for a new era," *Materials Today*, vol. 20, no. 3, pp. 142–154, 2017.

[2] M. A. Muñoz-Morris and D. G. Morris, "Microstructure and mechanical behaviour of a Fe-Ni-Al alloy," *Materials Science and Engineering, A*, vol. 444, no. 1-2, pp. 236–241, 2007.

[3] C. Stallybrass, A. Schneider, and G. Sauthoff, "The strengthening effect of (Ni,Fe)Al precipitates on the mechanical properties at high temperatures of ferritic Fe-Al-Ni-Cr alloys," *Intermetallics*, vol. 13, no. 12, pp. 1263–1268, 2005.

[4] Z. Teng, G. Ghosh, M. Miller et al., "Neutron-diffraction study and modeling of the lattice parameters of a NiAl-precipitate-strengthened Fe-based alloy," *Acta Materialia*, vol. 60, no. 13-14, pp. 5362–5369, 2012.

[5] Z. Sun, C. H. Liebscher, S. Huang et al., "New design aspects of creep-resistant NiAl-strengthened ferritic alloys," *Scripta Materialia*, vol. 68, no. 6, pp. 384–388, 2013.

[6] C. Stallybrass and G. Sauthoff, "Ferritic Fe-Al-Ni-Cr alloys with coherent precipitates for high-temperature applications," *Materials Science and Engineering A*, vol. 387–389, no. 1-2, pp. 985–990, 2004.

[7] S. Huang, Y. Gao, K. An et al., "Deformation mechanisms in a precipitation-strengthened ferritic superalloy revealed by in situ neutron diffraction studies at elevated temperatures," *Acta Materialia*, vol. 83, pp. 137–148, 2015.

[8] C. Liebscher, V. Radmilović, U. Dahmen et al., "A hierarchical microstructure due to chemical ordering in the bcc lattice: Early stages of formation in a ferritic Fe–Al–Cr–Ni–Ti alloy," *Acta Materialia*, vol. 92, pp. 220–232, 2015.

[9] N. Q. Vo, C. H. Liebscher, M. J. S. Rawlings, M. Asta, and D. C. Dunand, "Creep properties and microstructure of a precipitation-strengthened ferritic Fe-Al-Ni-Cr alloy," *Acta Materialia*, vol. 71, pp. 89–99, 2014.

[10] Z. Jiao, J. Luan, Z. Zhang, M. Miller, and C. Liu, "High-strength steels hardened mainly by nanoscale NiAl precipitates," *Scripta Materialia*, vol. 87, pp. 45–48, 2014.

[11] F. Yin, C. Wu, Z. Li, M. Zhao, and Y. Liu, "Phase Equilibrium of the Fe-Cr-Ni-Al Quarternary System at 900^{o}C," *Journal of Phase Equibria and Diffusion*, vol. 34, no. 3, pp. 181–187, 2013.

[12] Y. Zhao, Q. Fang, Y. Liu, P. Wen, and Y. Liu, "Creep behaiour as dislocation climb over NiAl nanoprecipitates in ferritic alloys: The effects of interface stresses and temperature," *International Journal of Plasticity*, vol. 69, pp. 89–101, 2015.

[13] P. Kofstad, "High temperature corrosion," in *Materials at High Temperatures Corrosion and Anti-Corrosives*, vol. 558, Elsevier Applied Science Publishers Ltd, 1988.

[14] P. Tomaszewicz and G. R. Wallwork, *The oxidation of high-purity iron-chromium-aluminium alloys at 800^{o}C, Oxidation of Metals*, vol. 20, article no. 75, 1983.

[15] H. J. Dorantes-Rosales, *Precipitation Process in Fe-Ni-Al-based Alloys*, Instituto Politcnico Nacional (ESIQIE-CNMN), Mexico, 2015.

[16] P. J. Ennis and W. J. Quadakkers, "Implications of steam oxidation for the service life of high-strength martensitic steel components in high-temperature plant," *International Journal of Pressure Vessels and Piping*, vol. 84, no. 1-2, pp. 82–87, 2007.

[17] E. Essuman, G. H. Meier, J. Zurek, M. Hänsel, L. Singheiser, and W. J. Quadakkers, "Enhanced internal oxidation as trigger for breakaway oxidation of Fe-Cr alloys in gases containing water vapor," *Scripta Materialia*, vol. 67, no. 9, pp. 845–848, 2007.

[18] N. Othman, N. Othman, J. Zhang, and D. Young, "Effects of water vapour on isothermal oxidation of chromia-forming alloys in Ar/O_2 and Ar/H_2 atmospheres," *Corrosion Science*, vol. 51, no. 12, pp. 3039–3049, 2009.

[19] M. P. Taylor, H. E. Evans, S. Stekovic, and M. C. Hardy, "The oxidation characteristics of the nickel-based superalloy, RR1000, at temperatures of 700–900°C," *Materials at High Temperatures*, vol. 29, no. 2, pp. 145–150, 2012.

[20] T. Dudziak, M. Witkowska, W. Ratuszek, and K. Chrusciel, "XRD phase investigations of steam oxidized Fe and Ni rich Cr alloys," *Transactions of Foundry Research Institure*, vol. LVII, no. 4, pp. 265–276, 2017.

[21] M. Bensch, A. Sato, N. Warnken, E. Affeldt, R. C. Reed, and U. Glatzel, "Modelling of high temperature oxidation of alumina-forming single-crystal nickel-base superalloys," *Acta Materialia*, vol. 60, no. 15, pp. 5468–5480, 2012.

[22] P. Kofstad, *High Temperature Corrosion, First Edition, Materials at high temperatures corrosion and anti-corrosives*, Elsevier Applied Science Publishers Ltd, Barking, UK, 1988.